Available online at www.sciencedirect.com

ScienceDirect

Advances in Space Research xxx (2017) xxx–xxx

ADVANCES IN SPACE RESEARCH (a COSPAR publication)

www.elsevier.com/locate/asr

Ozone chemical equilibrium in the extended mesopause under the nighttime conditions

M.V. Belikovich [a,*], M.Yu. Kulikov [a], M. Grygalashvyly [b], G.R. Sonnemann [b], T.S. Ermakova [a], A.A. Nechaev [a], A.M. Feigin [a,c]

[a] Institute of Applied Physics of the Russian Academy of Sciences, 46 Ulyanov Str., 603950 Nizhny Novgorod, Russia
[b] Leibniz-Institute of Atmospheric Physics at the University Rostock in Kühlungsborn, Schloss-Str. 6, 18225 Ostseebad Kühlungsborn, Germany
[c] Lobachevsky State University of Nizhni Novgorod, 23 Prospekt Gagarina, 603950 Nizhny Novgorod, Russia

Received 29 May 2017; received in revised form 29 September 2017; accepted 5 October 2017

Abstract

For retrieval of atomic oxygen and atomic hydrogen via ozone observations in the extended mesopause region (~70–100 km) under nighttime conditions, an assumption on photochemical equilibrium of ozone is often used in research. In this work, an assumption on chemical equilibrium of ozone near mesopause region during nighttime is proofed. We examine 3D chemistry-transport model (CTM) annual calculations and determine the ratio between the correct (modeled) distributions of the O_3 density and its equilibrium values depending on the altitude, latitude, and season.

The results show that the retrieval of atomic oxygen and atomic hydrogen distributions using an assumption on ozone chemical equilibrium may lead to large errors below ~81–87 km. We give simple and clear semi-empirical criterion for practical utilization of the lower boundary of the area with ozone's chemical equilibrium near mesopause.

Keywords: Middle atmosphere; Composition and structure; Chemistry; Measurements; Modeling

1. Introduction

It is hard to deny that atomic hydrogen and atomic oxygen are essential minor chemical constituents in mesosphere-lower thermosphere region because they are chemically active, and involved in thermal and radiative processes of the MLT. Furthermore, they take part in the formation of emission layers. The relation of atomic oxygen with transient luminous events was found recently (Wu et al., 2017). Unfortunately, in situ rocket-borne measurements of O and H are very limited (e.g., Hedin et al., 2009). More commonly, an atomic oxygen and atomic hydrogen distributions are investigated in the MLT by satellite measurements (Russell and Lowe, 2003; Mlynczak et al., 2007, 2013a, 2013b, 2014; Smith et al., 2010; Siskind et al., 2008, 2015). These observations are based on two assumptions concerning: (1) ozone's chemical equilibrium (hereafter OCE) and (2) the main processes entered into the balance equation.

The single reaction of photochemical ozone formation is the three-body reaction of molecular and atomic oxygens $O_2 + O + M \rightarrow O_3 + M$, where M is the air number density. Without a doubt, the main loss process of ozone near

* Corresponding author.
E-mail addresses: belikovich@ipfran.ru (M.V. Belikovich), kulm@appl.sci-nnov.ru (M.Yu. Kulikov), gryga@iap-kborn.de (M. Grygalashvyly), sonnemann@iap-kborn.de (G.R. Sonnemann), taalika@mail.ru (T.S. Ermakova), ant.a.nech@gmail.com (A.A. Nechaev), feigin@ipfran.ru (A.M. Feigin).

https://doi.org/10.1016/j.asr.2017.10.010
0273-1177/

mesopause region during the night is the reaction with atomic hydrogen, $O_3 + H \rightarrow O_2 + OH$. The reaction of ozone with atomic oxygen amounts to less than 10% of the total ozone loss and can be ignored (Smith et al., 2008). All other common for mesopause ozone balance reactions are even less important. In mesopause region ozone additionally reacts with OH, HO_2, NO, and NO_2. Assuming typical mesopause temperature 298 K one may assess corresponding reaction rates, which are $7.3 \cdot 10^{-14}$, $1.9 \cdot 10^{-15}$, $1.8 \cdot 10^{-14}$, and $3.2 \cdot 10^{-17}$ [cm^3 $molecule^{-1}$ s^{-1}], respectively (Table A.3.1, Brasseur and Solomon, 2005). Multiplying by maximal concentrations at 80–100 km (Table A.6.2, Brasseur and Solomon, 2005) we obtain loss rates $\sim 2.3 \cdot 10^{-7}$, $2.3 \cdot 10^{-9}$, $5.9 \cdot 10^{-7}$, and $3.5 \cdot 10^{-12}$ [s^{-1}], respectively, which are several orders lower than corresponding loss rate of the main reaction $7 \cdot 10^{-3}$ [s^{-1}]. Losses by reactions with Cl, Br, F are even less important due to lack of these chemical compounds in the mesopause (Shimazaki, 1985; Brasseur and Solomon, 2005). Thus, the second assumption is roughly valid for nighttime conditions. An applicability of the OCE assumption, for nighttime conditions is not as obvious, although it is of importance for other applications.

For several decades, OCE assumption has been used to study hydroxyl emission mechanisms, morphology, and variability in the extended mesopause region (Marsh et al., 2006; Xu et al., 2010, 2012; Kowalewski et al., 2014). Kulikov et al. (2006, 2009) proposed methods for the simultaneous retrieval of O, H, HO_2 and H_2O by joint OH and O_3 satellite measurements, where OCE assumption has been utilized. Mlynczak and Solomon (1991, 1993) and Mlynczak et al. (2013b) used this assumption to derive exothermic chemical heat. The OCE assumption was applied in order to study the mesospheric OH^* layer response to gravity waves (Swenson and Gardner, 1998). It is also applied in ultimately theoretical works (e.g. Grygalashvyly et al., 2014; Grygalashvyly, 2015). OCE assumption is used to derive the dependence of excited hydroxyl layer number density and altitude of atomic oxygen and temperature. Sonnemann et al. (2015), used it to analyze annual variations of OH^* layer. Very often this assumption is applied implicitly, when authors are equating the nighttime loss of ozone in reaction with atomic hydrogen and production of ozone by 3-body reaction of molecular and atomic oxygen (e.g., Nikoukar et al., 2007). However, except for several particular cases with rather narrow ranges of coordinates and local times (e.g., Smith and Marsh, 2005), the feasibility of these assumptions depending on time and coordinates has not been proved hitherto. Moreover, current knowledge regarding the chemistry of the MLT suggests that the lower boundary of applicability of the OCE can take place higher than 80 km. First, at 80 km, the concentration of H possesses considerable diurnal photochemical variations and during the night can decrease by approximately one order which leads to the corresponding growth of the characteristic time of ozone (Allen et al., 1984). Second, in the height range between 80 and 90 km, the photochemical system, and consequently ozone evolution, is essentially nonlinear (Konovalov and Feigin, 2000). In particular, in a nighttime phase space of the system, there are areas where characteristic ozone evolution time can be comparable to photochemical lifetime of ozone, which is equal to the invers loss term of ozone (Shimazaki, 1985; Brasseur and Solomon, 2005). From the physical point of view, obviously in such a case the condition of OCE will not be satisfied, and its application for the estimation of O and H via ozone and airglow measurements can lead to larger errors up to several orders. In this current paper we perform a global study of the OCE for the nighttime extended mesopause region based on 3D CTM. We calculate the relationship of "true" O_3 concentration to local equilibrium values O_{3eq} depending on height, latitude, and season. The paper is structured as follows: in the next chapter, the model is described; chapter three presents the results and discussion of our calculations; followed by concluding remarks in the last chapter.

2. Model and calculations

We use for our calculations the global 3D chemistry-transport model (CTM) of the middle atmosphere designed at the Leibniz Institute of Atmospheric Physics (IAP) particularly to study the spatio-temporal phenomena in the MLT region with focus on the extended mesopause region. Model calculates 3D advective and vertical diffusive transport (turbulent and molecular). The grid-point model extends from the ground up to 150 km (118 pressure-height levels). The horizontal resolution amounts to 5.625° latitudinally and 5.625° longitudinally. The chemistry module consists of 19 constituents, 49 chemical reactions and 14 photo-dissociation reactions. The chemical part has been described in numerous papers (e.g., Sonnemann et al., 1998; Körner and Sonnemann, 2001; Grygalashvyly et al., 2009, 2011, 2012). The CTM was validated with measurements, and particularly for ozone, in a number of papers (Hartogh et al., 2004, 2011; Sonnemann et al., 2006a, 2006b, 2007). Three-dimensional fields of the temperature and winds are used from the Canadian Middle Atmosphere Model (CMAM) (de Grandpre et al., 2000; Fomichev et al., 2002; Scinocca et al., 2008). We utilize dynamics and temperature of extended version of CMAM30-SD for year 2000 (http://climate-modelling.canada.ca/climatemodeldata/cmam/output/CMAM−Ext/CMAM30-SD/6hr/atmos/index.shtml).

We calculate the annual variation of the spatio-temporal distributions of the ratio

$$R = O_3/O_{3\,eq} \quad (1)$$

where O_3 are the ozone values calculated by the model, and $O_{3\,eq}$ are the values of ozone in photochemical equilibrium. The values of $O_{3\,eq}$ are calculated as a ratio of production to the reduced loss terms, which take into account all main sources and sinks:

Please cite this article in press as: Belikovich, M.V., et al. Ozone chemical equilibrium in the extended mesopause under the nighttime conditions. Adv. Space Res. (2017), https://doi.org/10.1016/j.asr.2017.10.010

$$O_{3\,eq} = \frac{k_9 \cdot O \cdot O_2 \cdot M}{k_{12} \cdot H + k_{10} \cdot O + k_{13} \cdot OH + k_{16} \cdot HO_2 + k_7 \cdot NO + k_8 \cdot NO_2}, \quad (2)$$

where k_i are the corresponding reaction rates (the reactions noted in the paper are given in Table 1), and 3D distributions of all other minor chemical constituents are taken from model calculations. Then we calculate $\overline{R} = N^{-1}\sum_{i=1}^{N} R_i$ (N – number of grid points through the nights for one month, and it is different for each latitude and height) the night time averaged monthly mean of R and standard deviation $\sigma_{eq} = \sqrt{\sum_{i=1}^{N}(R_i - \overline{R})^2/N}$ of this ratio for each month. Note that for retrieving O and H by SABER measurements, data were used at $\chi > 95°$ (e.g., Mlynczak et al., 2014). Similarly, in order to remove transition regions of sunset and sunrise, we take into account local time for which the solar zenith angle $\chi > 100°$. The works based on satellite measurements most often show the results on so-called pseudo altitudes. Following these, in the present paper we represent our results on pressure height (or so-called pseudo altitude) $z^* = -H\ln(p/p_0)$, where $H = 7$ km is the scale height, p is the pressure, and $p_0 = 1013$ hPa is the pressure at the surface.

3. Results and discussion

Fig. 1 shows height–latitude cross-sections for the ratio R (Eq. (1)) for each month. The dashed area corresponds to $\chi < 100°$. The white area represents the ratio out of interval [0.5, 1.5]. We assume that the OCE is valid if jointly are satisfied the following imbalances:

$$\begin{cases} 100\% \cdot |R - 1| \leqslant 10\%, \\ 100\% \cdot \sigma_{eq} \leqslant 10\%. \end{cases} \quad (3)$$

In other words, two criteria have to be jointly satisfied: (1) R lies between 0.9 and 1.1; (2) σ_{eq} is less than 0.1. Black solid lines in Fig. 1 mark the border of equilibrium z_{eq} – the lower border of the area where, according to (3), local values of ozone are expected to be in agreement with their equilibrium values. The magenta dashed line depicts peak of hydroxyl concentration. Note, that it follows well the seasonal-latitudinal variation of z_{eq}, 3–4 km beneath. This fact will be discussed below. Local irregularities beneath main z_{eq} are excluded. The ozone in the photochemical equilibrium is at the height $z_{eq} \leq z \leq 100$ km. The border of equilibrium z_{eq} depends on the season and latitude and varies in the interval ~82–92 km. During the summer months at middle and high latitudes z_{eq} amounts to ~90 km. The lowest altitudes of the border of equilibrium amount to ~82 km at low and middle latitudes. In the spring and fall seasons, the highest altitudes of z_{eq} are placed at high southern and northern latitudes, respectively. During winter months (e.g., January and February) ozone at high northern latitudes strongly deviated from its equilibrium especially during major and minor Sudden Stratospheric Warming (SSW) events. Generally, seasonal-latitudinal behavior of ozone and, consequently, R is determined by residual circulation and corresponding fluxes of atomic oxygen (downward in winter and upward in summer) and can be different from year to year.

Table 1
List of reactions.

(1) $O + OH + M \rightarrow HO_2 + M$	(10) $O + O_3 \rightarrow 2O_2$
(2) $H + HO_2 \rightarrow O_2 + H_2$	(11) $O + O + M \rightarrow O_2 + M$
(3) $OH + HO_2 \rightarrow O_2 + H_2O$	(12) $O_3 + H \rightarrow O_2 + OH$
(4) $O + OH \rightarrow O_2 + H$	(13) $O_3 + OH \rightarrow O_2 + HO_2$
(5) $O + HO_2 \rightarrow O_2 + OH$	(14) $H + HO_2 \rightarrow 2OH$
(6) $O_2 + H + M \rightarrow HO_2 + M$	(15) $OH + OH \rightarrow O + H_2O$
(7) $O_3 + NO \rightarrow NO_2 + O_2$	(16) $O_3 + HO_2 \rightarrow 2O_2 + OH$
(8) $O_3 + NO_2 \rightarrow O_2 + NO_3$	(17) $OH + H + M \rightarrow H_2O + M$
(9) $O + O_2 + M \rightarrow O_3 + M$	(18) $H + HO_2 \rightarrow H_2O + O$

Fig. 2 illustrates standard deviation of calculated R from its mean value, calculated at every latitude-altitude grid point. Generally, relative deviation of R ratio from one (Fig. 1) and standard deviation shown in Fig. 2 are correlated, as expected, i.e., the closer the ratio R is to 1, the smaller corresponding standard deviation of calculated R from its mean values.

The calculations show that the lower boundary of the area, where OCE is well satisfied, depends on latitude and annual variation. Thus, for the practical application of OCE assumption, it is necessary either to take into consideration only the area of heights over ~90 km or to find the criterion allowing on the basis of initial experimental data to identify a correctness of OCE locally.

If $\tau_{O_3} < \tau_{O_3\,eq}$, where τ_{O_3} is photochemical lifetime of ozone and $\tau_{O_3\,eq}$ is characteristic time of $O_{3\,eq}$, then ozone concentration follows the changes of its equilibrium (i.e., $O_3/O_{3\,eq} \cong 1$). If $\tau_{O_3} > \tau_{O_3\,eq}$, the concentration of ozone lags behind the asymptotic equilibrium $O_{3\,eq}$; thus, local differences between O_3 and $O_{3\,eq}$ may reach larger values. At altitudes z, slightly higher than z_{eq} ($z > z_{eq}$), it is almost always valid $\tau_{O_3} < \tau_{O_3\,eq}$, and at noticeable higher altitudes than threshold height ($z \gg z_{eq}$), it is valid $\tau_{O_3} \ll \tau_{O_3\,eq}$. Therefore, as a first approximation, weak inequality can be used ($\tau_{O_3} < \tau_{O_3\,eq}$).

As noted above, OH concentration peak mirrors the lower boundary of the O_3 equilibrium, at 3–4 km beneath. It is well known that OH^* layer is placed 3–4 km higher than the OH-layer during the night (Sonnemann et al., 2015). Thus, for the first approximation peak of excited hydroxyl emission (which is observed by satellites) may serve as a marker for the lower boundary of region where O_3 is in chemical equilibrium. The ozone is in chemical equilibrium at the exited hydroxyl layer altitude and above, while the equilibrium is violated below this border.

Hydroxyl and excited hydroxyl layers possess essential latitudinal and seasonal variations resulting from the interaction of the active minor chemical constituents and the variation of their principle sources, i.e., water vapor and ozone. The variations of temperature, eddy diffusion, wave,

Please cite this article in press as: Belikovich, M.V., et al. Ozone chemical equilibrium in the extended mesopause under the nighttime conditions. Adv. Space Res. (2017), https://doi.org/10.1016/j.asr.2017.10.010

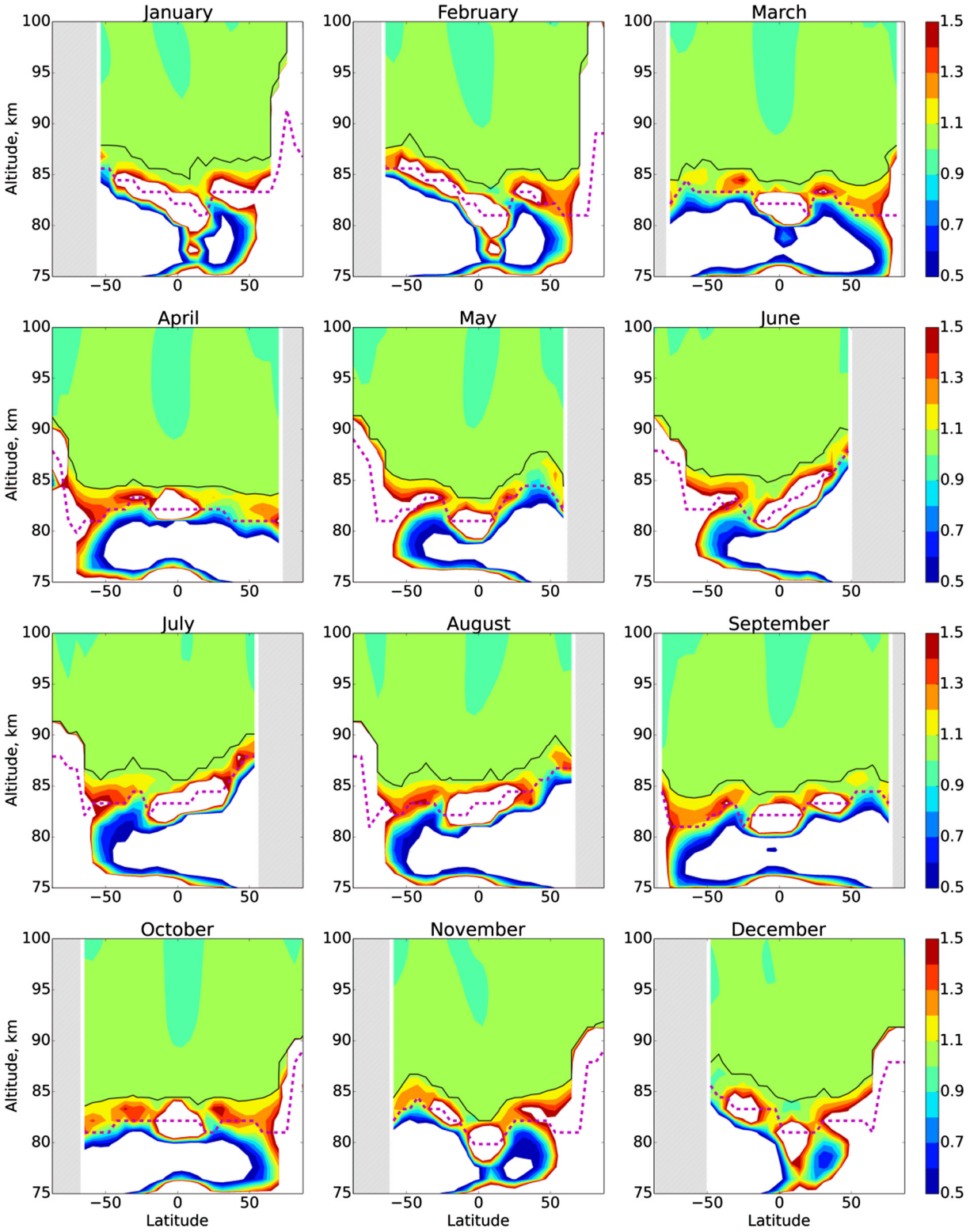

Fig. 1. Night time averaged monthly mean ratio O_3/O_{3eq} distributions. Black solid lines mark the border of equilibrium z_{eq}, the magenta dashed line depicts peak of OH concentration.

and tidal activity also interplay with them. The water vapor dissociation is the principle net production term of odd hydrogens. The oxidation of molecular hydrogen and water vapor by $O(^1D)$ produced by the ozone dissociation are of no importance in the mesopause region during the night. The vertical fluxes of O and H, however, play an important role in the chemistry of the mesopause region. The main production terms determining concentrations of hydroxyl are the reactions T12 and to a lesser degree, the reaction T5 and T16. The main destruction of hydroxyl

Please cite this article in press as: Belikovich, M.V., et al. Ozone chemical equilibrium in the extended mesopause under the nighttime conditions. Adv. Space Res. (2017), https://doi.org/10.1016/j.asr.2017.10.010

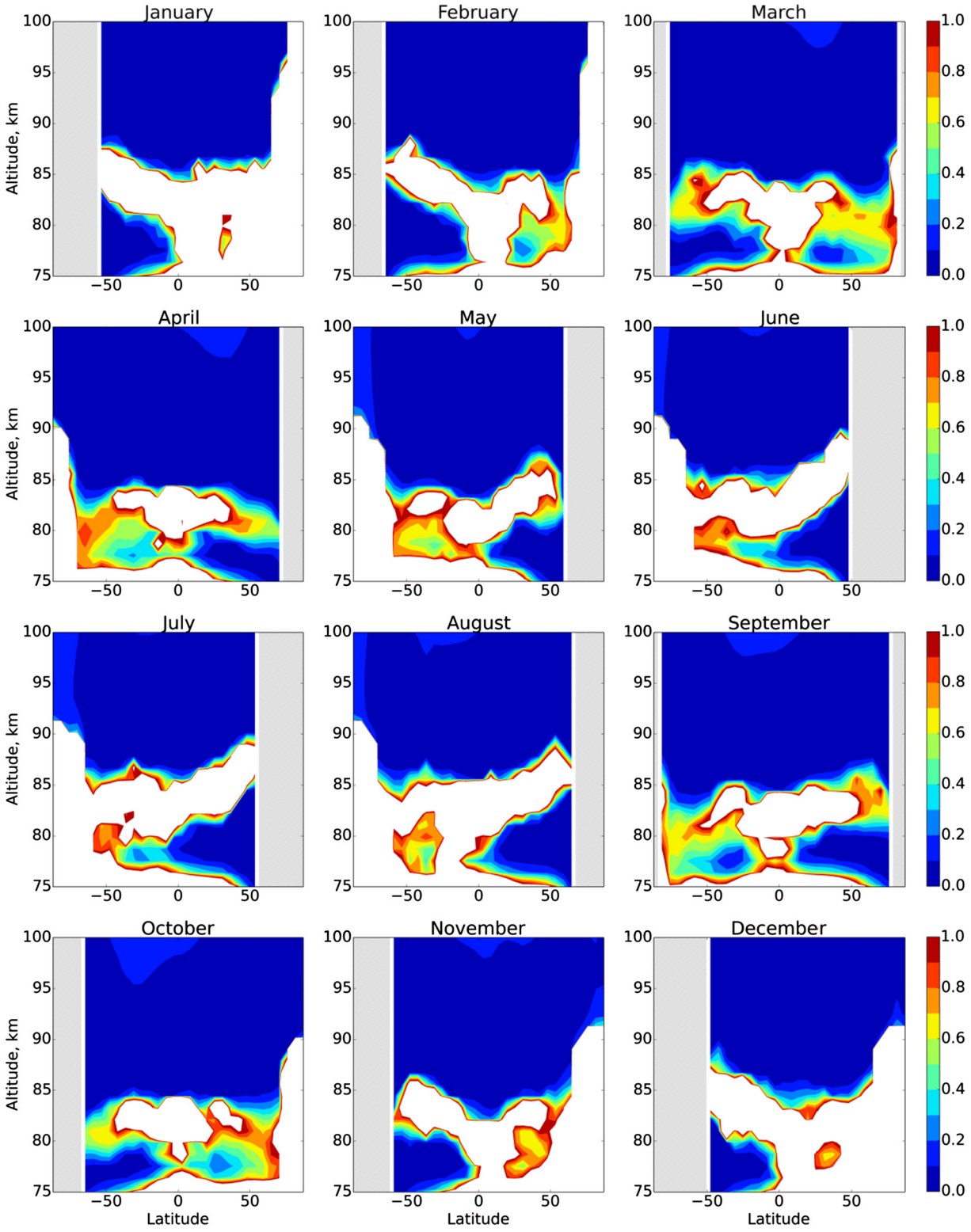

Fig. 2. Standard deviation σ_{eq} distributions of night time averaged monthly mean ratio $O_3/O_{3\,eq}$.

takes place by the T4. The chief reactions, determining the odd oxygen destroying catalytic cycle, are T12, T4, followed by the net reaction $O + O_3 \rightarrow 2\ O_2$. Thus, OH concentration is, approximately

$$[OH] \approx k_{12}[H][O_3]/k_4[O], \quad (4)$$

where k_{12} and k_4 are the corresponding reaction rates. Consequently, the Eq. (4) illustrates that the OH concentration depends on the concentration of the other important chemical active constituents, which are H, O, and O_3. The chemical lifetime of hydroxyl is extremely short (in the order of

Please cite this article in press as: Belikovich, M.V., et al. Ozone chemical equilibrium in the extended mesopause under the nighttime conditions. Adv. Space Res. (2017), https://doi.org/10.1016/j.asr.2017.10.010

seconds or even shorter), so that the hydroxyl is in a dynamic steady-state equilibrium following immediately the changing concentration of the involved constituents.

On the other hand, the reaction of ozone with atomic hydrogen is the most important ozone loss term around mesopause during the nighttime and primary production source for excited hydroxyl. Hence, it is not surprising that the strongest destruction of ozone occurs at the region of the OH^* layer. Thus, for practical usage the emission layer of excited hydroxyl may serve as the lower border of area with ozone under equilibrium condition. More detailed analyses of the application of these criteria need considerations of each particular measurement.

4. Conclusion

In the present work, the correctness of assumption of ozone chemical equilibrium in the extended mesopause region (70–100 km) during nighttime hours based on the results of 3D modeling was proved. We find that ozone concentrations are in photochemical equilibrium above 82–92 km depending on season and latitude. The ozone strongly deviated from its equilibrium beneath this border. We found by 3D simulation that the excited hydroxyl layer well repeat variability of the lower border of the ozone equilibrium area. Hence, peak of OH^* emission can be utilized for satellite observations as the boundary, which demarcates the area where OCE assumption is valid.

Acknowledgments

This work was supported by the Russian Science Foundation (contract No. 15–17–10024 of June 04, 2015). The data used in this study are supported by Institute of Applied Physics of the Russian Academy of Sciences (Nizhny Novgorod, Russia) and inquiries about calculated distributions used for this paper can be addressed to Mr. Belikovich (belikovich@ipfran.ru). The authors are thankful to Prof. Dr. F.-J. Luebken (Leibniz Institute of Atmospheric Physics, Kühlungsborn, Germany) for CTM-IAP model. Authors are grateful to two anonymous referees for constructive recommendations and improving suggestions.

References

Allen, M., Lunine, J.I., Yung, Y.L., 1984. The vertical distribution of ozone in the mesosphere and lower thermosphere. J. Geophys. Res. 89 (D3), 4841–4872.

Brasseur, G., Solomon, S., 2005. Aeronomy of the Middle Atmosphere: Chemistry and Physics of the Stratosphere and Mesosphere, third revised and enlarged edition. Springer, Dordrecht, The Netherlands.

Fomichev, V.I., Ward, W.E., Beagley, S.R., McLandress, C., McConnell, J.C., McFarlane, N.A., Shepherd, T.G., 2002. Extended Canadian middle atmosphere model: zonal-mean climatology and physical parameterizations. J. Geophys. Res. 107 (D10). https://doi.org/10.1029/2001JD000479.

de Grandpre, J., Beagley, S.R., Fomichev, V.I., Griffioen, E., McConnell, J.C., Medvedev, A.S., Shepherd, T.G., 2000. Ozone climatology using interactive chemistry: Results from the Canadian Middle Atmosphere Model. J. Geophys. Res. 105, 26475–26491.

Grygalashvyly, M., 2015. Several notes on the OH^* layer. Ann. Geophys. 33, 923–930. https://doi.org/10.5194/angeo-33-923-2015.

Grygalashvyly, M., Sonnemann, G.R., Hartogh, P., 2009. Long-term behavior of the concentration of the minor constituents in the mesosphere—A model study. Atmos. Chem. Phys. 9, 2779–2792. https://doi.org/10.5194/acp-9-2779-2009.

Grygalashvyly, M., Becker, E., Sonnemann, G.R., 2011. Wave mixing effects on minor chemical constituents in the MLT region: Results from a global CTM driven by high-resolution dynamics. J. Geophys. Res. 116, D18302. https://doi.org/10.1029/2010JD015518.

Grygalashvyly, M., Becker, E., Sonnemann, G.R., 2012. Gravity wave mixing and effective diffusivity for minor chemical constituents in the mesosphere/lower thermosphere. Space Sci. Rev. 168, 333–362. https://doi.org/10.1007/s11214-011-9857-x.

Grygalashvyly, M., Sonnemann, G.R., Lübken, F.-J., Hartogh, P., Berger, U., 2014. Hydroxyl layer: Mean state and trends at midlatitudes. J. Geophys. Res. 119, 12391–12419. https://doi.org/10.1002/2014JD022094.

Hartogh, P., Jarchow, C., Sonnemann, G.R., Grygalashvyly, M., 2004. On the spatiotemporal behavior of ozone within the upper mesosphere/mesopause region under nearly polar night conditions. J. Geophys. Res. 109, D18303. https://doi.org/10.1029/2004JD004576.

Hartogh, P., Sonnemann, G.R., Grygalashvyly, M., Jarchow, Ch., 2011. Ozone trends in mid-latitude stratopause region based on microwave measurements at Lindau (51.66° N, 10.13° E), the ozone reference model, and model calculations. Adv. Space Res. 47, 1937–1948. https://doi.org/10.1016/j.asr.2011.01.010.

Hedin, J., Gumbel, J., Stegman, J., Witt, G., 2009. Use of O_2 airglow for calibrating direct atomic oxygen measurements from sounding rockets. Atmos. Meas. Tech. 2, 801–812. https://doi.org/10.5194/amt-2-801-2009.

Körner, U., Sonnemann, G.R., 2001. Global 3D-modeling of water vapor concentration of the mesosphere/mesopause region and implications with respect to the NLC region. J. Geophys. Res. 106, 9639–9651.

Konovalov, I.B., Feigin, A.M., 2000. Towards an understanding of the non-linear nature of atmospheric photochemistry: origin of the complicated dynamic behavior of the mesospheric photochemical system. Nonlin. Processes Geophys. 7, 87–104.

Kowalewski, S., Savigny, C.v., Palm, M., McDade, I.C., Notholt, J., 2014. On the impact of the temporal variability of the collisional quenching process on the mesospheric OH emission layer: a study based on SD-WACCM4 and SABER. Atmos. Chem. Phys. 14, 10193–10210. https://doi.org/10.5194/acp-14-10193-2014.

Kulikov, M.Y., Feigin, A.M., Sonnemann, G.R., 2006. Retrieval of the vertical distribution of chemical components in the mesosphere from simultaneous measurements of ozone and hydroxyl distributions. Radiophys. Quantum Electron. 49, 683–691. https://doi.org/10.1007/s11141-006-0103-4.

Kulikov, M.Yu., Feigin, A.M., Sonnemann, G.R., 2009. Retrieval of water vapor profile in the mesosphere from satellite ozone and hydroxyl measurements by the basic dynamic model of mesospheric photochemical system. Atmos. Chem. Phys. 9, 8199–8210. https://doi.org/10.5194/acp-9-8199-2009.

Marsh, D.R., Smith, A.K., Mlynczak, M.G., Russell III, J.M., 2006. SABER observations of the OH Meinel airglow variability near the mesopause. J. Geophys. Res. 111, A10S05. https://doi.org/10.1029/2005JA011451.

Mlynczak, M.G., Solomon, S., 1991. Middle atmosphere heating by exothermic chemical reactions involving odd-hydrogen species. Geophys. Res. Lett. 18, 37–40.

Mlynczak, M.G., Solomon, S., 1993. A detailed evaluation of the heating efficiency in the middle atmosphere. J. Geophys. Res. 98, 10517–10541. https://doi.org/10.1029/93JD00315.

Mlynczak, M.G., Marshall, B.T., Martin-Torres, F.J., Russell III, J.M., Thompson, R.E., Remsberg, E.E., Gordley, L.L., 2007. Sounding of the Atmosphere using Broadband Emission Radiometry observations

of daytime mesospheric $O_2(^1D)$ 1.27 μm emission and derivation of ozone, atomic oxygen, and solar and chemical energy deposition rates. J. Geophys. Res. 112, D15306. https://doi.org/10.1029/2006JD008355.

Mlynczak, M.G., Hunt, L.A., Mast, J.C., Marshall, B.T., Russell III, J. M., Smith, A.K., Siskind, D.E., Yee, J.-H., Mertens, C.J., Martin-Torres, F.J., Thompson, R.E., Drob, D.P., Gordley, L.L., 2013a. Atomic oxygen in the mesosphere and lower thermosphere derived from SABER: Algorithm theoretical basis and measurement uncertainty. J. Geophys. Res. 118, 5724–5735. https://doi.org/10.1002/jgrd.50401.

Mlynczak, M.G., Hunt, L.H., Mertens, C.J., Marshall, B.T., Russell III, J. M., López-Puertas, M., Smith, A.K., Siskind, D.E., Mast, J.C., Thompson, R.E., Gordley, L.L., 2013b. Radiative and energetic constraints on the global annual mean atomic oxygen concentration in the mesopause region. J. Geophys. Res. Atmos. 118, 5796–5802. https://doi.org/10.1002/jgrd.50400.

Mlynczak, M.G., Hunt, L.A., Marshall, B.T., Mertens, C.J., Marsh, D.R., Smith, A.K., Russell, J.M., Siskind, D.E., Gordley, L.L., 2014. Atomic hydrogen in the mesopause region derived from SABER: Algorithm theoretical basis, measurement uncertainty, and results. J. Geophys. Res. 119, 3516–3526. https://doi.org/10.1002/2013JD021263.

Nikoukar, R., Swenson, G.R., Liu, A.Z., Kamalabadi, F., 2007. On the variability of mesospheric OH emission profiles. J. Geophys. Res. 112, D19109. https://doi.org/10.1029/2007JD008601.

Russell, J.P., Lowe, R.P., 2003. Atomic oxygen profiles (80–94 km) derived from Wind Imaging Interferometer/Upper Atmospheric Research Satellite measurements of the hydroxyl airglow: 1. Validation of technique. J. Geophys. Res. 108 (D21), 4662. https://doi.org/10.1029/2003JD003454.

Scinocca, J.F., McFarlane, N.A., Lazare, M., Li, J., Plummer, D., 2008. The CCCma third generation AGCM and its extension into the middle atmosphere. Atmos. Chem. Phys. 8 (7055–7074), 2008. https://doi.org/10.5194/acp-8-7055-2008.

Shimazaki, T., 1985. Minor constituents in the middle atmosphere. D. Reidel Publishing Company, Dordrecht, Holland.

Siskind, D.E., Marsh, D.R., Mlynczak, M.G., Martin-Torres, F.J., Russell III, J.M., 2008. Decreases in atomic hydrogen over the summer pole: Evidence for dehydration from polar mesospheric clouds? Geophys. Res. Lett. 35, L13809. https://doi.org/10.1029/2008GL033742.

Siskind, D.E., Mlynczak, M.G., Marshall, T., Friedrich, M., Gumbel, J., 2015. Implications of odd oxygen observations by the TIMED/SABER instrument for lower D region ionospheric modeling. J. Atmos. Sol. Terr. Phys. 124, 63–70.

Smith, A.K., Marsh, D.R., 2005. Processes that account for the ozone maximum at the mesopause. J. Geophys. Res. 110, D23305. https://doi.org/10.1029/2005JD006298.

Smith, A.K., Marsh, D.R., Russell III, J.M., Mlynczak, M.G., Martin Torres, F.J., Kyrölä, E., 2008. Satellite observations of high nighttime ozone at the equatorial mesopause. J. Geophys. Res. 113 (D17312), 2008. https://doi.org/10.1029/2008JD010066.

Smith, A.K., Marsh, D.R., Mlynczak, M.G., Mast, J.C., 2010. Temporal variations of atomic oxygen in the upper mesosphere from SABER. J. Geophys. Res. 115, D18309. https://doi.org/10.1029/2009JD013434.

Sonnemann, G., Kremp, C., Ebel, A., Berger, U., 1998. A three-dimensional dynamic model of minor constituents of the mesosphere. Atmos. Environ. 32, 3157–3172. https://doi.org/10.1016/S1352-2310(98)00113-7.

Sonnemann, G.R., Grygalashvyly, M., Hartogh, P., Jarchow, C., 2006a. Behavior of mesospheric ozone under nearly polar night conditions. Adv. Space Res. 38, 2402–2407.

Sonnemann, G.R., Hartogh, P., Jarchow, C., Grygalashvyly, M., Berger, U., 2006b. The winter anomaly of the night-to-day ratio of ozone in the middle to upper mesosphere in middle latitudes: A comparison between measurements and model calculations. Adv. Geosci. 9, 177–190.

Sonnemann, G.R., Hartogh, P., Jarchow, C., Grygalashvyly, M., Berger, U., 2007. On the winter anomaly of the night-to-day ratio of ozone in the middle to upper mesosphere in middle to high latitudes. Adv. Space Res. 40, 846–854.

Sonnemann, G.R., Hartogh, P., Berger, U., Grygalashvyly, M., 2015. Hydroxyl layer: trend of number density and intra-annual variability. Ann. Geophys. 33, 749–767. https://doi.org/10.5194/angeo-33-749-2015.

Swenson, G.R., Gardner, C.S., 1998. Analytical models for the responses of the mesospheric OH^* and Na layers to atmospheric gravity waves. J. Geophys. Res. 103 (D6), 6271–6294. https://doi.org/10.1029/97JD02985.

Wu, Y.J., Williams, E., Chang, S.C., Chou, J.K., Hsu, R.R., Friedrich, M., Kuo, C.L., Chen, A.B., Peng, K.M., Su, H.T., Frey, H.U., Mende, S.B., Takahashi, Y., Lee, L.C., 2017. The leading role of atomic oxygen in the collocation of elves and hydroxyl nightglow in the low-latitude mesosphere. J. Geophys. Res. 122. https://doi.org/10.1002/2016JA023681.

Xu, J., Smith, A.K., Jiang, G., Gao, H., Wei, Y., Mlynczak, M.G., Russell III, J.M., 2010. Strong longitudinal variations in the OH nightglow. Geophys. Res. Lett. 37, L21801. https://doi.org/10.1029/2010GL043972.

Xu, J., Gao, H., Smith, A.K., Zhu, Y., 2012. Using TIMED/SABER nightglow observations to investigate hydroxyl emission mechanisms in the mesopause region. J. Geophys. Res. 117, D02301. https://doi.org/10.1029/2011JD016342.

Please cite this article in press as: Belikovich, M.V., et al. Ozone chemical equilibrium in the extended mesopause under the nighttime conditions. Adv. Space Res. (2017), https://doi.org/10.1016/j.asr.2017.10.010